Computation of object approach by a system of visual motion-sensitive neurons in the crab *Neohelice*

Damián Oliva and Daniel Tomsic

J Neurophysiol 112:1477-1490, 2014. First published 3 June 2014; doi:10.1152/jn.00921.2013

J Neurophysiol 112: 1477–1490, 2014.
First published June 4, 2014; doi:10.1152/jn.00921.2013.

Computation of object approach by a system of visual motion-sensitive neurons in the crab *Neohelice*

Damián Oliva[1] and Daniel Tomsic[2]

[1]*Departamento de Ciencia y Tecnología, Universidad Nacional de Quilmes, CONICET, Buenos Aires, Argentina; and* [2]*Laboratorio de Neurobiología de la Memoria, Departamento Fisiología, Biología Molecular y Celular, Facultad de Ciencias Exactas y Naturales, Universidad de Buenos Aires, IFIBYNE-CONICET, Buenos Aires, Argentina*

Submitted 31 December 2013; accepted in final form 30 May 2014

Oliva D, Tomsic D. Computation of object approach by a system of visual motion-sensitive neurons in the crab *Neohelice*. *J Neurophysiol* 112: 1477–1490, 2014. First published June 4, 2014; doi:10.1152/jn.00921.2013.—Similar to most visual animals, crabs perform proper avoidance responses to objects directly approaching them. The monostratified lobula giant neurons of type 1 (MLG1) of crabs constitute an ensemble of 14–16 bilateral pairs of motion-detecting neurons projecting from the lobula (third optic neuropile) to the midbrain, with receptive fields that are distributed over the extensive visual field of the animal's eye. Considering the crab *Neohelice* (previously *Chasmagnathus*) *granulata*, here we describe the response of these neurons to looming stimuli that simulate objects approaching the animal on a collision course. We found that the peak firing time of MLG1 acts as an angular threshold detector signaling, with a delay of $\delta = 35$ ms, the time at which an object reaches a fixed angular threshold of 49°. Using in vivo intracellular recordings, we detected the existence of excitatory and inhibitory synaptic currents that shape the neural response. Other functional features identified in the MLG1 neurons were phasic responses at the beginning of the approach, a relation between the stimulus angular velocity and the excitation delay, and a mapping between membrane potential and firing frequency. Using this information, we propose a biophysical model of the mechanisms that regulate the encoding of looming stimuli. Furthermore, we found that the parameter encoded by the MLG1 firing frequency during the approach is the stimulus angular velocity. The proposed model fits the experimental results and predicts the neural response to a qualitatively different stimulus. Based on these and previous results, we propose that the MLG1 neuron system acts as a directional coding system for collision avoidance.

looming; collision avoidance; motion detection; lobula neurons; receptive field; crustacean

MOST VISUAL ANIMALS ARE HIGHLY effective at detecting and avoiding collisions, which may occur either by encounters with obstacles during navigation (Tammero and Dickinson 2002; Srinivasan and Zhang 2004) or by moving objects, such as predators, that directly approach them (Rind and Simmons 1999; Fotowat and Gabbiani 2011; Card 2012). In both cases, an important visual cue to predict a potential collision is the image expansion of the approaching surface or object from a particular direction, known as the looming stimulus. The detection of this visual cue triggers motor programs controlled by neural circuits to generate quick and reliable avoidance responses, which range from ballistic-like behaviors (Glantz 1974a; Tammero and Dickinson 2002) to more complex behaviors, such as multistage avoidance responses (Fotowat and Gabbiani 2007; Hemmi 2005a), and continually regulated systems to the observed changes in the approaching stimulus direction and speed (Land and Layne 1995; Oliva and Tomsic 2012). To be effective, the avoidance maneuvers must be executed in a timely and accurate manner, which implies that the approaching object must be precisely monitored in real time. Thus most animals possess movement detector neurons that are specially tuned to detect objects approaching on a collision course. Neurons tightly tuned to detect these stimuli, called looming-sensitive neurons (LSNs), have been identified in arthropods, such as locusts (Schlotterer 1977; Rind and Simmons 1992; Gabbiani et al. 1999; Gray et al. 2010), flies (Borst 1991; Fotowat et al. 2009), praying mantis (Yamawaki and Toh 2009), crayfish (Glantz 1974a), and crabs (Oliva et al. 2007; Medan et al. 2007).

The most important property of LSNs is their preferential response to looming rather than to receding, translating stimuli or whole-field motion. Furthermore, LSNs typically have weak directional sensitivity across their visual field (Krapp and Gabbiani 2005; Medan et al. 2007), respond to small object movements, and have large receptive fields (Rowell et al. 1977). Some LSNs have feed-forward inhibitory processes that increase with the size of the moving object, controlling the response saturation to looming stimuli (Rowell et al. 1977; Gabbiani et al. 1999). Another phenomenon observed in many LSNs is the response reduction to repetitive stimulation or habituation (Glantz 1974b; O'Shea and Rowell 1975; Tomsic et al. 2003; Gray 2005).

How do sensory circuits encoding looming stimuli work, and what are the biophysical processes that tune LSNs to looming stimuli? To date, the most complete answers to these questions have been obtained in the lobula giant movement detector (LGMD) neuron of the locust. The main conclusion has been that several biophysical processes operate in parallel to shape the visual response of the LGMD (reviewed in Oliva 2013). These processes include feed-forward excitation and feed-forward inhibition (Gabbiani et al. 1999), adaptation (Peron and Gabbiani 2009), lateral inhibition (Rind and Bramwell 1996), and synchronization (Jones and Gabbiani 2010).

Defensive and escape responses to looming stimuli have been extensively documented in crustaceans. For example, upon frontal looming, crayfish rise and open their claws at times related with the stimulus dynamic (Glantz 1974a) or may perform freezing or avoidance responses (Herberholz and Marquart 2012). In semiterrestrial crabs, avoidance responses to looming stimuli have been studied in the field (e.g., Hemmi 2005a,b) and in the laboratory (Oliva et al. 2007; Oliva and

Address for reprint requests and other correspondence: D. Oliva, Departamento de Ciencia y Tecnología, Universidad Nacional de Quilmes. Roque Sáenz Peña 352, Bernal. Buenos Aires, Argentina (B1876BXD) (e-mail: doliva@unq.edu.ar).

Tomsic 2012). These animals employ multistage predator avoidance strategies that include freezing, escaping, and defensive responses depending on the level of risk; different detector systems that are sensitive to different aspects of predator-associated visual cues may operate to assess this risk (Hemmi 2005b). Even the escape strategy is not a simple reflex; instead, it is a finely tuned, complex behavioral sequence that is modulated at all levels of organization (for a review, see Hemmi and Tomsic 2012). For example, in response to an approaching object, the direction and speed of the run are continuously adjusted according to ongoing visual information provided by the stimulus (Land and Layne 1995; Oliva and Tomsic 2012). Crabs must be suitably equipped with LSNs to accomplish these behaviors.

Motion-sensitive fibers of crustaceans were first studied by Wiersma et al. using extracellular recordings from the protocerebral tract (reviewed in Wiersma et al. 1982). In crayfish, movement-detector fibers appear to be the only cell type descending from the optic lobe with the appropriate response properties to trigger a defense reflex to looming stimuli (Glantz 1974b). More recently, the morphological identity of several classes of motion fibers has been established in the crab *Neohelice* using in vivo intracellular recording and staining. These neurons are generically named lobula giants (LGs) because, similar to the LGMD of the locust, their dendrites arborize extensively in the lobula and their axons project through the long protocerebral tract towards the midbrain. All LGs respond to object motion rather than to optic flow (Medan et al. 2007) and display habituation to repeated stimulation (Berón de Astrada and Tomsic 2002). However, according to their dendritic arborizations in the lobula, LGs have been divided into monostratified LG types 1 and 2 (MLG1 and MLG2) or bistratified LG types 1 and 2 (BLG1 and BLG2) (Medan et al. 2007). These different classes are also distinguished by the number of elements present in each class, the amount of binocular input they receive (Sztarker and Tomsic 2004), their receptive field properties, and their capacity to integrate visual with proprioceptive information from the legs (Berón de Astrada and Tomsic 2002; Medan et al. 2007). The responses of LG neurons to different visual danger stimuli in a variety of conditions have been found to anticipate and closely reflect the temporal course and intensity profile of the crab's escape response (Tomsic et al. 2003; Oliva et al. 2007; Sztarker and Tomsic 2008, 2011).

In particular, the classes MLG1 and MLG2 proved to be highly sensitive to looming stimuli and exhibit many of the properties that characterize the LSNs discussed above (Oliva et al. 2007). The MLG2 is a large neuron with a dendritic tree that extends over the entire retinotopic mosaic of the lobula and has a homogenous receptive field that encompasses the entire visual field of the animal (crabs have monocular vision of 360°). There is apparently only one MLG2 per lobula (Medan et al. 2007). In contrast, the MLG1 forms an ensemble of 14–16 units that are evenly distributed across the transversal axes of the lobula (the axes that maps the azimuth; Berón de Astrada et al. 2011), where each element has dendrites that collect information from a limited portion of the visual columnar mosaic (Sztarker et al. 2005). MLG1 neurons respond earlier than the MLG2 neuron and, in contrast to the MLG2 neuron, do not integrate visual with proprioreceptor information from the animal's legs (Medan et al. 2007). Therefore, MLG1 appears to be an earlier and simpler stage of looming information processing than MLG2. Thus here we focus our investigation in MLG1 neurons. Previous experiments (Oliva et al. 2007) used a single looming stimulus, which prevented the exploration of possible mechanisms involved in the coding of the stimuli. In this study, we characterized the response of MLG1 neurons with different looming dynamics, determined important parameters that shape their response, and propose a plausible biophysical model of the mechanisms that regulate the encoding of looming stimuli.

METHODS

Animals

Animals were adult male *Neohelice* (previously *Chasmagnathus*) *granulata* crabs, 2.7–3.0 cm across the carapace, weighing ~17 g. The crabs were collected in the rías (narrow coastal inlets) of San Clemente del Tuyú, Argentina and transported to the laboratory, where they were lodged in plastic tanks (35 × 48 × 27 cm) that were filled to a depth of 2 cm with diluted seawater to a density of 20 crabs per tank. The water used in the tanks and other containers during the experiments was prepared using hw-Marinex (Winex, Hamburg, Germany), salinity 10–14‰, pH 7.4–7.6, and maintained within a temperature range of 22–24°C. The holding and experimental rooms were maintained on a 12:12-h light-dark cycle (lights on from 0700 to 1900), and the experiments were performed between 0800 and 1900. Experiments were performed within the first 2 wk after the animal's arrival. Crabs were fed rabbit pellets (Nutrients, Buenos Aires, Argentina) every 3 days, and the water was changed after feeding. Experimental procedures were in compliance with the National Institutes of Health *Guide for the Care and Use of Laboratory Animals* and the Argentinian guidelines on the ethical use of animals. This work was approved by our research institution.

Visual Stimuli

Computer-generated visual stimuli were projected alternatively on three flat-screen monitors (Philips 107T; horizontal and vertical screen dimensions were 32 and 24 cm, respectively, with a refreshing rate of 60 Hz), located 20 cm in front of and on both sides of the animal (Fig. 1*A*). The monitors were completely covered to prevent outside visual stimuli from reaching the animal, and anti-glare screens reduced reflections among the monitors. The three monitors stood on a vibration-damped table. Electrophysiological experiments began after a black curtain was lowered in the front part of the cage and after the animal had remained visually undisturbed for 3 min. All visual stimuli were generated from one PC using commercial software (Presentation 5.3; Neurobehavioral Systems, Albany, CA). The frame rate of the rendered files was 60 Hz, i.e., it matched the refresh rate of the monitor. A range of different stimuli could then be selected and presented to different parts of the visual field without distressing the animal while neuronal activity was being recorded (Medan et al. 2007).

Visual simulations generated by computer may differ from the visual input experienced under natural conditions in various respects. For example, the refresh rate of a monitor screen may impose a severe constraint on the study of the visual system of animals with a high flicker fusion frequency. We did not measure the fusion frequency in *Neohelice*; however, in fiddler crabs, this frequency was found to be <50 Hz (Layne et al. 1997). In crayfish, responses to looming stimuli corresponding to real approaching objects or filmed representations projected at 24 frames/s yielded identical results (Glantz 1974b). The effectiveness of two-dimensional computer images to elicit the crab's escape response has previously been demonstrated in *Neohelice* (Oliva et al. 2007; Oliva and Tomsic 2012). Moreover, we found no differences between the escape response elicited by a black sheet of cardboard approaching the animal and the computer simulation of an object of the same size and approach speed (Oliva 2010).

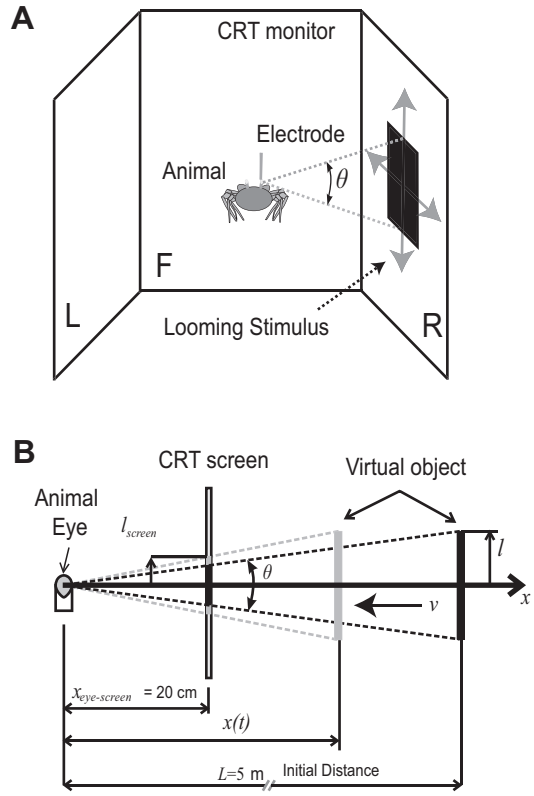

Fig. 1. Simulation of an object's approach at constant speed. *A*: computer-generated visual stimuli were projected alternatively on 3 flat-screen CRT monitors located 20 cm in front of and on both sides of the animal (R, right; F, front; L, left). *B*: virtual object at 2 different times. $x(t)$ is the position of the object in a reference system centered on the right eye of the crab, v is the speed of approach towards the crab, θ is the total angle subtended by the object at the eye of the crab, and l_{screen} is the apothem of the square drawn on the monitor screen.

Kinematics of Object Approach

The stimuli used simulated dark squares of various sizes approaching with constant speeds on a direct collision course towards the animal (Fig. 1*B*). Let l denote the object half-size. The distance between the animal eye and virtual object at time t is $x(t)$, and the object subtends an angle $\theta(t)$ on the eye. Thus we can write

$$\tan\left[\theta(t)/2\right] = \frac{l}{x(t)} \tag{1}$$

With the chosen coordinate system and time definitions, we have $x(t) \geq 0$, $t \geq 0$. Objects were simulated to start their approach from a distance $L = 5$ m. The position of the object is given by

$$x(t) = L - v \cdot t \tag{2}$$

where v is the absolute value of the approach speed.

The square drawn on the monitor screen (Fig. 1*B*) has a half-size $l_{screen}(t)$ and depends on the distance from the monitor to the eye of the animal, $x_{eye\text{-}screen}$, as follows:

$$\tan\left[\theta/2\right] = \frac{l_{screen}}{x_{eye-screen}} = \frac{l}{x(t)} \tag{3}$$

Replacing $x(t)$ from *Eq. 2* and solving for $l_{screen}(t)$, we obtain

$$l_{screen}(t) = \frac{x_{eye-screen} \cdot l}{x(t)} = \frac{x_{eye-screen} \cdot l}{L - v \cdot t} \tag{4}$$

Equation 4 describes a half-size square drawn on the screen monitor as a function of time. Due to the limits imposed by the screen's size and distance to the animal's eye, the maximum stimulus expansion was $\theta(t) = 60°$.

In the literature regarding looming detection, the dynamic of a stimulus expansion is typically characterized by the fraction l/v (Gabbiani et al. 1999). By replacing $x(t)$ from *Eq. 2* in *Eq. 3*, we obtain

$$\tan(\theta/2) = \frac{l}{L - v \cdot t} = \frac{1}{L/l - v \cdot t/l} = \frac{1}{1/\tan(\theta_0/2) - t/(l/v)} \tag{5}$$

Equation 5 indicates that each stimulus is characterized by a value of l/v and of θ_0.

The angular edge velocity of the object, $\Psi(t)$, is defined as

$$\psi(t) = \frac{\theta'}{2} = \frac{1}{2}\frac{d\theta}{dt}. \tag{6}$$

In the analysis of collision avoidance responses, it is common to use the "time to collision" (referred to as t_c) as a relevant variable. In this article, time to collision is given by:

$$t_c = T - t \tag{7}$$

where T is the travel time of the virtual object from its initial position until the time of collision.

Stimuli Used

We used a total of eight stimuli (Table 1). For *stimuli 1–4*, we maintained the approach speed $v = 142.5$ cm/s and varied the size l from 8.5 to 64 cm. The subtended angle of the smallest stimulus at the initial distance was 1.8°, which is above the sampling resolution of the crab's eye. In fact, in the lateral part of the eye, the resolution reaches values between 0.83 and 1.2 cycles/°, corresponding to interommatidial angles between 0.6 and 0.4°, respectively (Berón de Astrada et al. 2012). Thus animals would not have optical limitations to detect differences between the initial sizes of the smaller stimuli used here. For *stimuli 5–7*, we maintained $l = 17$ cm and varied v from 35.5 to 286 cm/s. These speeds attempted to simulate predators that approach the animal faster than its ability to run away (*Neohelice's* highest escape speed is 35 cm/s). Finally, we applied a qualitatively different stimulus consisting of a black square expanding at a constant angular velocity $\omega = \theta' = 7.4$°/s.

Conditions of Stimulation

In Oliva et al. (2007), we described features of the escape response and the optimal stimulation parameters, such as the interval between

Table 1. *Looming stimulus parameters (see Fig. 1)*

Stimulus No.	l, cm	v, cm/s	l/v (ms)	L, m	T, s	θ_0, °
1	8.5	142.5	56	5	3.5	1.8
2	17	142.5	120	5	3.5	3.9
3	32	142.5	225	5	3.5	7.3
4	64	142.5	450	5	3.5	14.5
5	17	35.5	479	5	14	3.9
6	17	71.5	238	5	7	3.9
7	17	286	60	5	1.75	3.9
8	Angular velocity $\omega = 7.4$ °/s				7	3.9

Looming stimulus parameters (*stimuli 1–7*): l is the half-size of the object, v is the approach speed, L is the initial distance, T is the travel time between the initial position to the collision, and θ_0 is the initial angular size of the object in degrees. The parameters l/v and θ_0 are used to describe the dynamics in terms of time to collision (see text). *Stimulus 8*: black square expands at a constant angular velocity $\omega = 7.4$°/s.

trials, the direction of approach, and the object contrast against the background. Based on those results, we began stimulation after the animal had remained visually undisturbed for 3 min inside the setup. In all trials, the stimulus remained stationary for 30 s at its initial position before starting to increase in size. The intertrial interval was set to 1 min. We used black squares expanding on a white background. Irradiance on the monitor screen was 4 mW/m^2 (black square) and 240 mW/m^2 (background). The eight stimuli in Table 1 were applied to each animal in a random order.

Electrophysiology

Intracellular recordings from interneurons in the optic lobe were performed in the intact living animal according to methods previously described (Berón de Astrada and Tomsic 2002). Briefly, the crab was firmly held in an adjustable clamp. The eyestalks were cemented to the carapace at an angle of ~70° from the horizontal line. A tangential cut performed with a sharp scalpel was made to remove a small piece of thin cuticle (~500 μm in diameter) from the tip of the right eyestalk without causing damage to the ommatidial area. The crab was positioned in the center of the arrangement of monitors (Fig. 1*A*) within the Faraday cage. The clamp with the crab was held in position using a magnetic holding device. The glass microelectrode was then positioned and advanced through the opening in the cuticle. Microelectrodes (borosilicate glass; 1.2-mm outer diameter, 0.68-mm inner diameter) were pulled on a Brown-Flaming micropipette puller (P-97; Sutter Instrument, Novato, CA) yielding tip resistances of 40–60 MΩ when filled with 3 mol/l KCl. A bridge balance amplifier was used for intracellular recordings (Axoclamp 2B; Axon Instruments, Union City, CA). The output of the amplifier was monitored on an analog oscilloscope, digitized at 10 kHz (Digidata 1320; Axon Instruments), and recorded on a computer for subsequent analysis. All intracellular recordings were performed at the membrane resting potential. The monitors located inside the Faraday cage generated a significant level of electrical noise in the recordings, but we were able to prevent the noise in two ways: *1*) by placing a wire mesh immediately in front of each screen, and *2*) by wrapping the headstage, the electroholder, and part of the glass electrode with a dense, properly grounded, metal wire mesh. During the experiment crabs intermittently moved their legs for a few seconds, which sometimes resulted in losing the impaled cell. These movements, however, did not appear to be associated in time with the presentation of the looming stimulus since they usually occurred within intertrials periods. Following electrophysiological recordings, crabs remained healthy and no subsequent behavioral differences were observed with respect to nontreated animals.

Classification Criteria for M1 Neurons

To determine the identity of each neuron recorded intracellularly, we used such properties as receptive field size, spontaneous activity, and response to a light pulse (Medan et al. 2007). MLG1 neurons are easy to identify; they have no spontaneous discharges and a phasic response to a flash of light. In this study, we recorded and analyzed 11 MLG1 neurons from different animals (no more than 2 trials per stimulus per neuron).

Data Analysis

We estimated the instantaneous firing rate by convolving the spike trains with a square window (width of 50–100 ms) and normalizing the resulting waveform such that its integral was equal to the total number of spikes over the entire trial (Gabbiani et al. 1999). To quantify the intensity of the MLG1 response to each monitor (Fig. 2), the standardized response r was defined as $r(n) = N_{spk}(n)/[N_{spk}(R) + N_{spk}(F) + N_{spk}(L)]$, where $n = \{R,F,L\}$ identifies the corresponding monitor. A least-squares linear regression was used for the linear fit (see Fig. 4). The parameters of the proposed model were estimated by nonlinear least-squares error minimization between the mean firing rate and model prediction. The uncertainties of the model parameters were estimated using the boostrap method (Wasserman 2004). Analysis procedures were written in Matlab (The MathWorks, Natick, MA). The model and code to generate the fits (see Figs. 8 and 9) and Supplemental Material for this article are available online at the *J Neurophsiol* website. Further details are provided in RESULTS.

RESULTS

Responses of MLG1 Neurons to Looming Stimuli from Different Approaching Directions

Medan et al. (2007) performed a preliminary characterization of the receptive field of MLG1 neurons using a black square (size 14°) stimulus with horizontal and vertical translational movements at a speed of 48°/s. The receptive field of

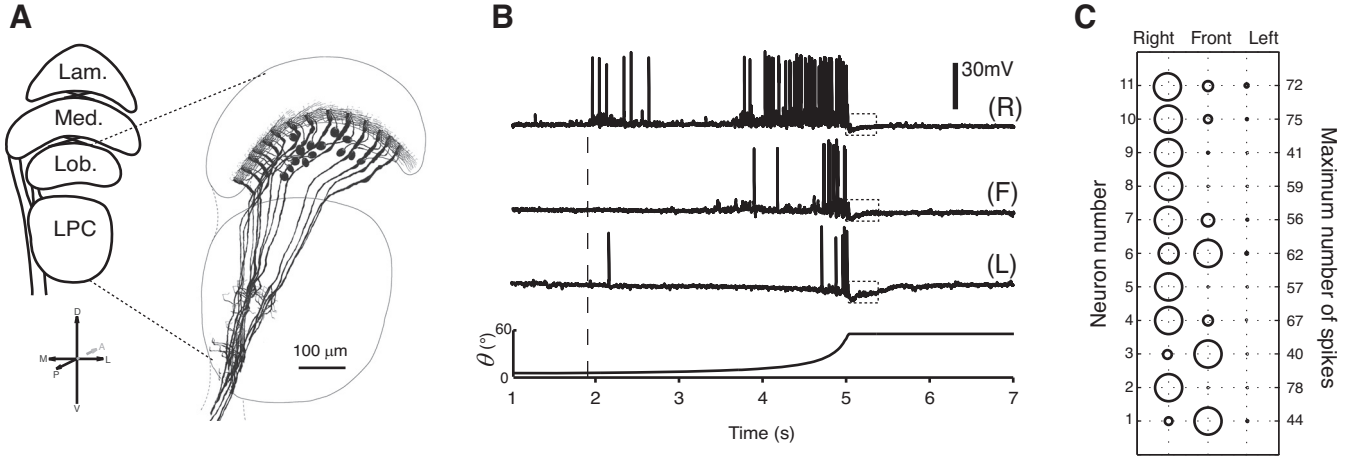

Fig. 2. Receptive field of monostratified lobula giant neurons of type 1 (MLG1) to looming stimuli. *A*: schematic representation of the arrangement of MLG1 neurons in the crab's lobula (from Medan 2008 with permission). Lamina (lam), medulla (med), lobula (lob), and lateral protocerebrum (LPC) are shown. The letters in the coordinate axes correspond to the following: D, dorsal; V, ventral; M, medial; L, lateral; A, anterior; P, posterior. *B*: responses of a MLG1 neuron to a looming stimulus (v = 142.5 cm/s, l = 17 cm) presented separately on the monitor to the right (R), front (F), and left (L) sides of the animal. The dashed line marks the beginning of the stimulus expansion. The lower curved line represents the time course of the stimulus image expansion. The dotted squares indicate the relaxation of the membrane potential after the end of the looming stimulus. *C*: normalized response magnitude to stimuli presented on the different monitors for 11 measured neurons. Numbers at *right* indicate the maximum number of spikes elicited by the stimulus in each neuron.

MLG1 neurons can be approximated by a Gaussian distribution with a standard deviation σ of 13° for neurons sampling the lateral visual pole (Medan 2008). Based on these data and on the fact that each MLG1 occupies a different position on the lobula retinotopic mosaic (Fig. 2*A*) (Sztarker et al. 2005), MLG1 neurons are expected to respond preferentially to looming stimuli approaching from a particular direction. As shown in the example in Fig. 2*B*, with the application of *stimulus 2* (Table 1) in the three monitors separately, the neuron responded preferentially to the right monitor (throughout the experiments recordings were performed from the right optic lobe). In this series of experiments, 8 out of 11 neurons (72%) had their receptive fields mainly located over the right monitor, although the receptive field was between two monitors in some cases. The other three neurons (28%) responded preferentially to stimuli located on the frontal monitor (Fig. 2*C*). More elements with receptive fields on the right side of the animal were recorded because impalements were most likely performed in the middle of the neuropil, a region of the lobula that maps the lateral visual field (Berón de Astrada et al. 2011).

Response of MLG1 Neurons to Different Dynamics of Approach

After finding the monitor with the maximum response for each neuron, we evaluated the response to the eight stimuli described in Table 1. For *stimuli 1–4* (Table 1), we maintained an approaching speed of $v = 142.5$ cm/s and changed the size of the object l from $l = 8.5$–64 cm. For *stimuli 5–7*, we maintained $l = 17$ cm while varying the speed of the object v from 35.5 to 286 cm/s. Finally, *stimulus 8* was a qualitatively different stimulus, with a constant angular velocity of expansion (7.4°/s).

Figure 3 presents the typical responses of an MLG1 neuron to looming stimuli. The response consists of a depolarization accompanied by spiking activity that progressively increases as the image of the virtual object grows over the retina of the animal. This increase in the spiking activity is followed by a subsequent decrease. The peak activity occurs before the expansion is completed (dotted circles). For a more detailed analysis, we plotted the mean peak firing time relative to the collision, $t_{c,peak} = T - t_{peak}$, as a function of l/v ($n = 11$ neurons). This plot revealed a relation that could be fitted by a linear function with slope α and intercept δ (Fig. 4). Therefore, this observation and the analyses developed by Gabbiani (see Fig. 5*A* in Gabbiani et al. 1999) indicate that MLG1 peak firing time acts as an angular threshold detector, signaling the time at which an object reaches a fixed angular size $\theta_{thres} = 2 \tan^{-1}(1/\alpha) = 49°$ on the retina with a delay of $\delta = 35$ ms.

Another feature observed in different recordings of MLG1 was the existence of a transient component of the response at

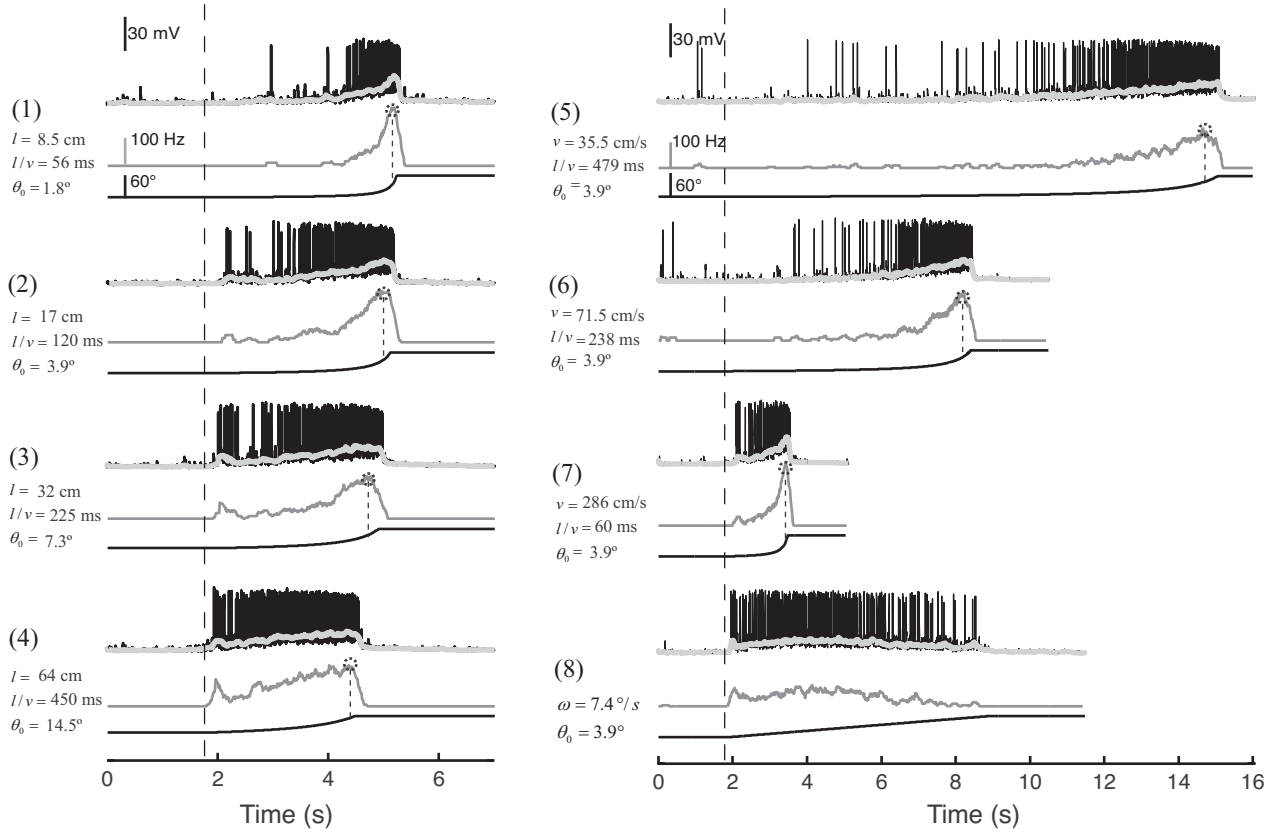

Fig. 3. Response of 1 MLG1 neuron to different looming stimuli. *Left*: responses to *stimuli 1–4*. *Right*: responses to *stimuli 5–8*. Intracellular recordings from a single MLG1 illustrate the type of responses of the neuron to the 8 different stimuli (black traces). To estimate the average of the membrane potential, we applied a median filter (width: 50 ms) to remove the action potentials (light gray traces, see METHODS for more details). Dark gray traces below correspond to the firing frequency after convolving the spike trains with a square window (see METHODS). Dotted circles on the top of the dotted lines correspond to the peak of the response. The time course of the stimulus image expansion is given at *bottom* (black curved line). Dashed vertical lines signal the beginning of the stimulus expansion. Numbers between brackets refer to stimuli numbers in Table 1. The 8 stimuli were applied to each animal in a random order. Intertrial interval = 1 min.

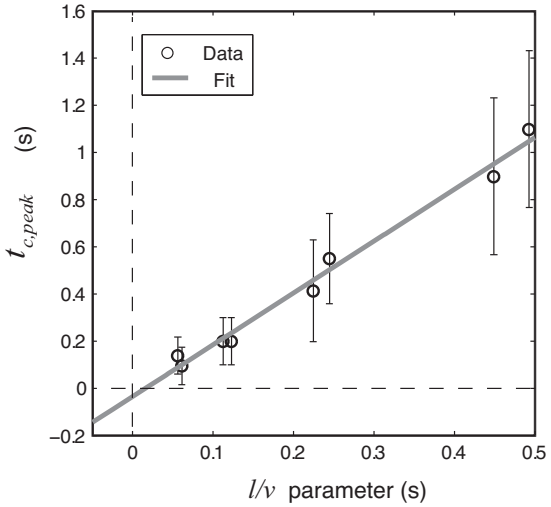

Fig. 4. Quantitative examination of the timing of the maximum responses of MLG1 neurons. Measurements of the time remaining to collision (absolute values) when the peak in firing rate was produced as a function of the looming parameter *l*/*v*. The relation between the time of peak firing rate ($t_{c,peak}$) and *l*/*v* is linear with $\alpha = 2.2 \pm 0.27$ and $\delta = -0.035 \pm 0.04$ s. This result indicates that MLG1 peak firing time acts as an angular threshold detector, signaling, with a delay of $\delta = 35$ ms, the time at which an object reaches a fixed angular size of 49°.

the beginning of the expansion (Rind and Simmons 1992). This effect can be observed in Fig. 3 mainly with *stimuli 3*, *4*, and *7* ($\theta_0 = 7.3$, 14.5, and 3.9°, respectively).

Excitatory and Inhibitory Synaptic Currents in MLG1 Neurons

One factor that can produce a maximum firing rate before the end of the expansion may be the limited size of the receptive field of the MLG1. Another possible factor can be the existence of an inhibitory process acting in parallel with presynaptic excitation (Gabbiani et al. 1999, 2002). Two pieces of evidence support the existence of synaptic inhibition acting on MLG1 neurons. First, when we applied a flash of light, an inhibitory response was often detected with or without previous spikes (Fig. 5*A*, dotted ellipses). Second, when presenting the looming stimulus on monitors where the MLG1 response was weak, we again observed inhibition without a previous production of spikes (Fig. 5*B*, see also Fig. 2*B*). From these observations, we propose that there is synaptic excitation and inhibition acting on the dendrites of the MLG1. As observed in the records, synaptic inhibition appears to have a reversal potential near the resting potential, a phenomenon known as shunting inhibition.

Relationship Between the Average Membrane Potential and Firing Frequency in MLG1 Neurons

Intracellular recordings were likely performed in the dendritic region near the spike initiation zone because the primary dendritic process of MLG1 neurons has an exceptionally wide diameter (Medan et al. 2007) and its orientation is perpendicular to the descending direction of the electrode (Sztarker et al. 2005). Figure 6 provides an example of an intracellular recording with noticeable synaptic activity and spikes backpropagated to the dendritic region. The intracellular recordings allowed us to analyze the relationship between the dendritic membrane potential and neuronal firing frequency. A cursory inspection of the records of Fig. 3 suggests a covariation between the value of the filtered membrane potential (light gray trace) and the firing rate (dark gray line). To obtain the filtered membrane potential, we applied a median filter (width of 50 ms) to remove the action potentials (Fig. 6*A*, see also Fig. 3). Then, we plotted the firing rate as a function of the filtered membrane potential and observed a clear mapping between the two variables that could be adjusted with a power law input-output function (Gabbiani et al. 2002):

$$R = k_r \cdot \left(V_{mf}\right)^{a_r} \quad (8)$$

where R is the firing rate, V_{mf} is the filtered membrane potential relative to the resting potential V_{rest}, and k_r and a_r are constants obtained for each neuron. Note that the exact fit function (particularly the exponent) is likely to depend on how far the recording location is from the spike initiation zone of the neuron. We fit the model of *Eq. 8* for different neurons ($n = 5$; $r^2 = 0.86$) to obtain: $k_r = 1.2 \pm 0.4$ Hz (means ± SD) and $a_r = 1.5 \pm 0.25$ (means ± SD).

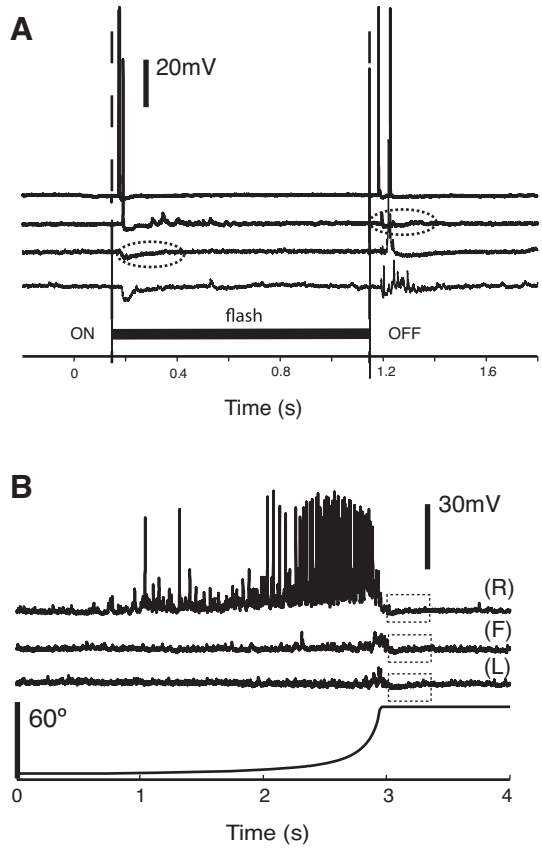

Fig. 5. Synaptic inhibition onto MLG1 neurons. *A*: response to a light pulse stimulus. Each trace corresponds to a response of a different neuron. MLG1 neurons have a phasic response to a light pulse. After a brief excitation that produces action potentials, an inhibitory postsynaptic potential can be observed. This inhibition can occur with or without the production of spikes, indicating it does not result from a spike rebound but has a synaptic origin. *B*: response to a looming stimulus in monitors R, F, and L. For responses to the F and L monitors, we observed a depolarization followed by an inhibition after the end of the expansion (with no previous production of spikes). The dotted squares indicate the approximate relaxation of the membrane potential after the end of the looming stimulus (see also Fig. 2*B*).

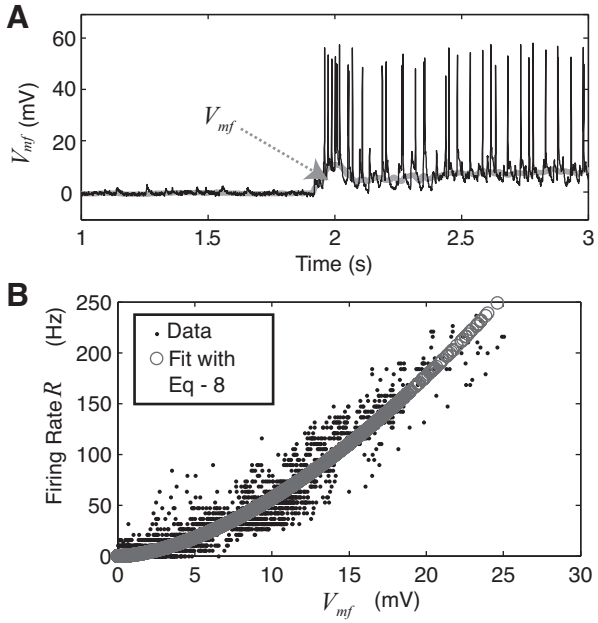

Fig. 6. Mapping between the filtered membrane potential and firing frequency. *A*: example of a MLG1 activity that illustrates the generation of action potentials and the dendritic membrane voltage V_m relative to V_{rest} (gray trace). The filtered membrane potential V_{mf} was obtained by median filtering with a time window of 50 ms. *B*: firing rate R as a function of the filtered membrane potential V_{mf}. Gray circles indicate the fit using *Eq. 8* for 1 neuron, to which the 8 stimuli in Table 1 were applied.

Dependence of the Excitation Latency on the Stimulus Angular Velocity

Recent studies have examined the response of the excitatory presynaptic circuit acting on the LGMD in photoreceptors and lamina monopolar cell (LMC) (Jones and Gabbiani 2010, 2012). The visual stimulus consisted of an edge moving at constant angular velocity Ψ through the receptive field of these neurons. Recordings from LMCs revealed that these neurons responded to these luminance changes with an increasing depolarization proportional to the edge's speed Ψ and consistent with the high-pass filtering properties reported in other insect species (Laughlin and Hardie 1978). Another observed effect was that the latency of the peak response in LMC cells decreased as the stimulus duration became shorter (or as the edge velocity, Ψ, was increased). Based on these results in LGMD neurons, a variation in the excitation latency δ_e between the beginning of the looming expansion and the onset of the MLG1 response is expected. In addition, this latency should be a function of the angular velocity of the moving edge at the beginning of the expansion (Fig. 7, *A* and *B*). This analysis was performed with eight MLG1 neurons with receptive fields mainly located over the right monitor (2 trials per stimulus, per neuron, per animal). We used *stimuli 2*, *3*, and *4* because these were the stimuli for which we clearly detected the onset of the neural response (Fig. 7). For each trial, δ_e is defined as the time interval between the beginning of the expansion and the onset of the neuronal response. The response onset was selected as the time when the firing rate exceeded twice the maximum rate reached in the 2 s before stimulation. Because the spontaneous firing of MLG1 is almost null (e.g., Fig. 3), in most cases the response onset corresponded to the first elicited spike. As shown in Fig. 7*C*, we found a relationship between the latency in the MLG1 response onset (in seconds) and the looming stimulus angular velocity (in degrees per second):

$$\delta_e = 0.5^{\circ}/(\theta' + 0.01) + 0.03 \quad (9)$$

This effect was considered in our proposed model for the synaptic excitation of MLG1 neurons.

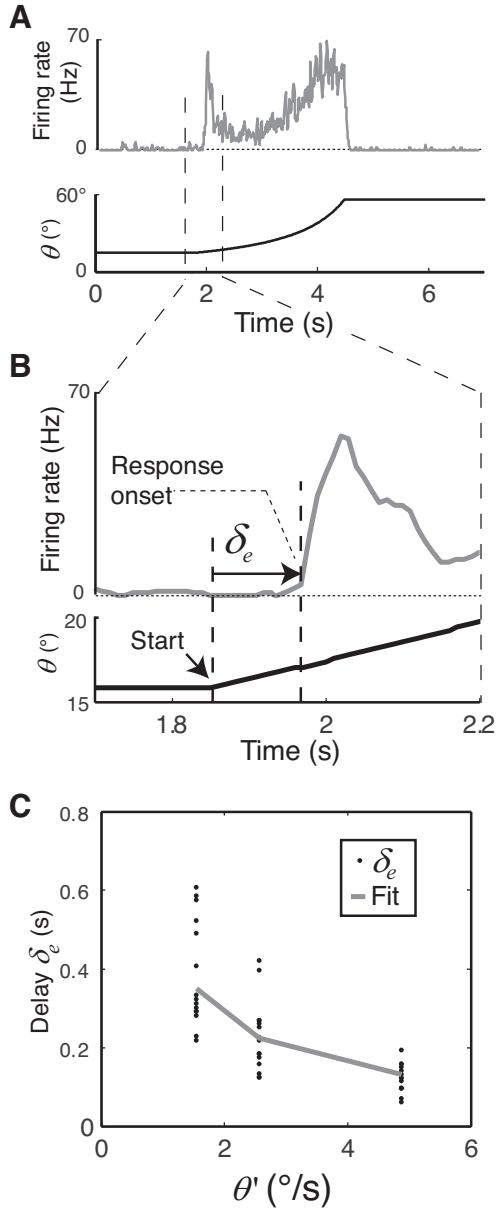

Fig. 7. Dependence of the mean excitation latency δ_e on the stimulus angular velocity. *A*: average firing frequency (gray trace) from 8 MLG1 neurons with receptive fields mainly located over the right monitor (2 trials per stimulus, per neuron, per animal). The black curved line represents the angular size of the stimulus $\theta(t)$ as a function of time for stimulus 4 (Table 1). *B*: delay measurement: δ_e is the time interval between the beginning of the expansion and the onset of the neuronal response. The response onset was selected at the time when the firing rate exceeded twice the maximum response in the 2 s before stimulation. *C*: average delay values (in seconds) as a function of the angular velocity at the response time (8 neurons from 8 different animals, 2 trials per cell). The delay decreased significantly with increasing edge speed $\Psi = \theta'/2$ (black circles). The gray trace illustrates the fit ($r^2 = 0.56$), with $\delta_e = 0.5°/(\theta' + 0.01) + 0.03$.

Model Assumptions and Approximations

A fundamental mechanism shaping the response of movement detector neurons consists of a dynamic balance between excitation and inhibition (Gabbiani et al. 1999; Weber et al. 2010). In vivo intracellular recording of MLG1 responses to light pulses and looming stimuli revealed the existence of excitatory and inhibitory inputs to this neuron (Fig. 5). Another effect that we considered in the model is that MLG1 neurons looking towards the lateral pole have a Gaussian receptive field with a standard deviation σ of 13°. Thus the size of the receptive field becomes important as the looming stimulus expands to 60°. Using the detailed computational models of the LGMD neuron (Rind and Bramwell 1996; Peron and Gabbiani 2009; Jones and Gabbiani 2012) as a guide, we introduced several simplified assumptions to fit our model to the measurements.

1) The expanding black edges move with angular velocity Ψ, and the photoreceptors have an on-off transition with a duration inversely proportional to Ψ (Jones and Gabbiani 2012) (Fig. 8*A*). The signal of columnar channels that impinge on the MLG1 is proportional to the activity of LMC neurons that can be approximated by

$$f_{\mathrm{LMC}}(\psi) = \left[\frac{\psi}{\psi_{\max}}\right]^{a_{\mathrm{LMC}}} \quad (10)$$

where a_{LMC} is a constant to be fitted and $\Psi_{\max}$ is selected to obtain an adimensional and normalized function f_{LMC}. For this purpose, its value was fixed as the maximum angular velocity for all stimuli, $\Psi_{\max} = 382°/\mathrm{s}$.

2) We approximated the surface of the eye around the focus of expansion as a planar surface (known as the "small angle approximation"). The coordinates (θ,φ) measured the azimuthal and longitudinal position, respectively (Fig. 8*A*). The reference system was chosen so that the focus of expansion (FOE) was centered at the origin $(\theta,\varphi) = (0,0)$.

Based on previous results (Medan et al. 2008), we propose a Gaussian receptive field for the angular sensitivity of MLG1 neurons (gray circular dashed lines in Fig. 8*A*):

$$C_{\mathrm{r}}(\theta,\varphi) = k_{\mathrm{RF}} \cdot \exp\left[-\frac{(\theta-\theta_{\mathrm{c}})^2 + (\varphi-\varphi_{\mathrm{c}})^2}{2\cdot\sigma^2}\right] \quad (11)$$

where k_{RF} is a proportionality constant, σ is the receptive field (RF) standard deviation, and $(\theta_{\mathrm{c}},\varphi_{\mathrm{c}})$ describes the center position of the RF relative to the FOE.

3) Based on previous work (Gabbiani et al. 2001) and using the planar approximation to the surface of the eye, we propose that the presynaptic signal acting on the MLG1 neuron during the image frame $(t,\ t+\Delta t)$ is proportional to *a*) the number of ommatidia with an on-off transition weighed by the value of the receptive field $C_{\mathrm{r}}(\theta,\varphi)$ of the neuron along the expanding border, and *b*) the intensity of LMC response described by $f_{\mathrm{LMC}}(\Psi)$:

$$\mathrm{pre}(t) = k_{\mathrm{pre}} \cdot \left[\oint_{Ce} \mathrm{dl}_{Ce} \cdot C_r(\theta,\varphi)\right] \cdot \psi(t) \cdot \Delta t \cdot f_{\mathrm{LMC}}[\psi(t)] \quad (12)$$

where k_{pre} is an adimensional constant selected such that the pre(t) signal was normalized to the maximum value reached

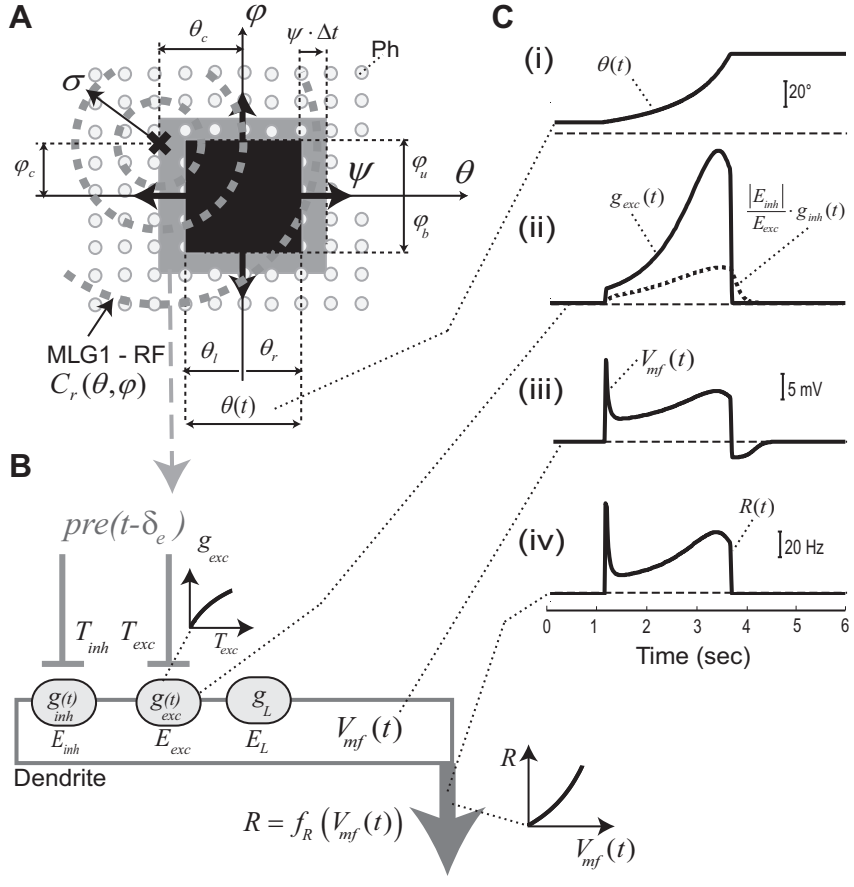

Fig. 8. Plausible biophysical model of looming detection in MLG1 neurons. *A*: expanding black edges move in the horizontal and vertical directions (θ,φ) with an angular velocity Ψ through the ommatidial array (small light gray circles). In every monitor's new frame, the square increases its angular size, $\theta(t)$ (gray square). The MLG1 receptive field (C_{r}) is indicated as gray dashed circles, and its center is displaced $(\theta_{\mathrm{c}},\varphi_{\mathrm{c}})$ relative to the focus of expansion located at the origin of the reference *system* $(\theta,\varphi) = (0,0)$. Every new frame, the angular size is increased by $2\Psi\cdot\Delta t$, changing the upper, lower, left, and right edges positions, φ_{u}, φ_{b}, θ_{l}, and θ_{r}, respectively. *B*: proposed model assumes that when the figure is expanded, the signal of presynaptic columnar channels, pre$(t-\delta_{\mathrm{e}})$, activates excitatory and inhibitory synapses with conductance (g_{exc}, g_{inh}) acting on the dendrites of the neuron MLG1. The dynamic balance between these conductances determines the filtered membrane voltage, V_{mf} according to *Eq. 15*. Finally, the firing rate *R* is calculated using *Eq. 8*. *C*: example of the temporal evolution of the model variables. *i*: Angular size, $\theta(t)$, as a function of time for *stimulus 4* (see Table 1). *ii*: Excitatory and inhibitory conductances, $g_{\mathrm{exc}}(t)$ and $g_{\mathrm{inh}}(t)$, vs. time. The inhibitory conductance, $g_{\mathrm{inh}}(t)$, was normalized to illustrate its relative weight in the evolution of V_{mf} (see *Eq. 15*). *iii*: Estimation of the filtered membrane potential, V_{mf}. *iv*: Prediction of the firing rate using *Eq. 8*.

with *stimulus 1* (which is the maximum value obtained for all stimuli).

Furthermore:

$$\oint_{Ce} \mathrm{d}l_{Ce} \cdot C_\mathrm{r}(\theta, \varphi) = \int_{\theta_l}^{\theta_r} \left[C_\mathrm{r}(\theta, \varphi_\mathrm{b}) + C_\mathrm{r}(\theta, \varphi_\mathrm{u})\right] \cdot \mathrm{d}\theta + \int_{\phi_\mathrm{b}}^{\phi_\mathrm{u}} \left[C_\mathrm{r}(\theta_l, \varphi) + C_\mathrm{r}(\theta_\mathrm{r}, \varphi)\right] \cdot \mathrm{d}\varphi$$

corresponds to a line integral along the expanding border. This integral is divided into two terms: the first, corresponds to the contribution of the horizontal edges (top and bottom), located at the angles φ_u and φ_b, respectively. The second term relates to the contribution of the vertical edges (left and right, respectively), located at the angles θ_l and θ_r (Fig. 8*A*).

4) Based on the results in Figs. 2 and 5, we suggest that there are two pathways acting presynaptically on neuron MLG1: a fast excitatory pathway (modeled as first-order dynamics with low-pass filter $\tau_\mathrm{exc} = 10$ ms) and a slow inhibitory pathway (with $\tau_\mathrm{inh} = 100$ ms; Fig. 8*B*). Then,

$$\begin{aligned} \tau_\mathrm{exc} \cdot \frac{\mathrm{d}T_\mathrm{exc}}{\mathrm{d}t} + T_\mathrm{exc} &= \mathrm{pre}(t - \delta_e) \\ \tau_\mathrm{inh} \cdot \frac{\mathrm{d}T_\mathrm{inh}}{\mathrm{d}t} + T_\mathrm{inh} &= \mathrm{pre}(t - \delta_e) \end{aligned} \quad (13)$$

where T_exc and T_inh are proportional to the concentration of the neurotransmitter released at the presynaptic space and the excitation latency δ_e is modeled according to *Eq. 9* (Fig. 7*C*).

5) We assumed that the neurotransmitter (T_exc, T_inh) released reacted with receptors (R_exc, R_inh) according to first-order dynamics (Destexhe et al. 1994). We further assumed that the neurotransmitter instantly reached the steady state. Therefore, the postsynaptic conductances are proportional to the amount of neurotransmitter released as follows:

$$\begin{aligned} g_\mathrm{exc}(t) &= g_\mathrm{e,max} \cdot \frac{T_\mathrm{exc}(t)}{T_\mathrm{exc,50\%} + T_\mathrm{exc}(t)} \\ g_\mathrm{inh}(t) &= g_\mathrm{i,max} \cdot \frac{T_{inh}(t)}{T_\mathrm{inh,50\%} + T_\mathrm{inh}(t)} \end{aligned} \quad (14)$$

where $g_\mathrm{e,max}$ and $g_\mathrm{i,max}$ are the maximum conductances associated with total excitatory and inhibitory synapses, respectively. The parameters $T_\mathrm{exc,50\%}$ and $T_\mathrm{inh,50\%}$ are the values of the variables $T_\mathrm{exc}(t)$ and $T_\mathrm{inh}(t)$ when $g_\mathrm{exc}(t)$ and $g_\mathrm{inh}(t)$ reach 50% of $g_\mathrm{e,max}$ and $g_\mathrm{i,max}$, respectively.

6) Finally, we assumed that because the temporal evolution of the conductances is slower than the characteristic time of the membrane potential, we can approximate the filtered membrane potential to its steady state:

$$V_\mathrm{mf}(t) = \frac{\left(g_\mathrm{exc}(t)/g_L\right) \cdot E_\mathrm{exc} + \left(g_\mathrm{inh}(t)/g_\mathrm{L}\right) \cdot E_\mathrm{inh} + E_\mathrm{L}}{\left(g_\mathrm{exc}(t)/g_\mathrm{L}\right) + \left(g_\mathrm{inh}(t)/g_\mathrm{L}\right) + 1} \quad (15)$$

where g_L is the leak conductance and E_L, E_exc, and E_inh are the leak, excitatory, and inhibitory reverse potentials, respectively. Thus *Eq. 15* provides an approximate expression for the evolution of a filtered dendritic membrane potential, and the firing rate can be calculated using *Eq. 8*.

In summary, the model variables were calculated as follows (Fig. 8*C*): from the angular size $\theta(t - \delta_\mathrm{e})$, the angular edge's velocity $\Psi = \theta'(t - \delta_\mathrm{e})/2$, and the latency δ_e (obtained from *Eq. 9*), we calculated the presynaptic signal $\mathrm{pre}(t - \delta_\mathrm{e})$ using *Eqs. 10–12*. Integrating *Eq. 13* with the Euler method and using *Eq. 14*, we calculated the excitatory and inhibitory conductances (Fig. 8*Cii*). Finally, we obtained the filtered membrane potential, V_mf, using *Eq. 15* (Fig. 8*Ciii*) and the firing rate R using *Eq. 8* (Fig. 8*Civ*).

Parameter Selection and Model Fit

The next objective was to fit the proposed model to the MLG1 average response using neurons with a maximum response to the right monitor (see Fig. 2). Based on intracellular recording and considering the resting membrane potential $E_\mathrm{l} = 0$ mV, we assumed the following values: excitatory synaptic reversal potential $E_\mathrm{exc} = 60$ mV, inhibitory synaptic reversal potential $E_\mathrm{inh} = -3$ mV; excitatory time constant $\tau_\mathrm{exc} = 10$ ms; inhibitory time constant $\tau_\mathrm{inh} = 100$ ms; firing rate exponent $a_\mathrm{r} = 1.5$; parameter $k_\mathrm{r} = 1.2$; and RF standard deviation $\sigma = 13°$.

The signal $\mathrm{pre}(t)$ was normalized to the maximum value reached with *stimulus 1*. To meet this condition, the adimensional constant k_pre should be $k_\mathrm{pre} = 0.012$. Finally, the proportionality constant k_RF, was assumed to be $k_\mathrm{RF} = 1\ \mathrm{deg}^{-2}$.

Parameters that could not be approximated using intracellular recording information were estimated by nonlinear square error minimization between the mean firing rate and model prediction. We used *stimuli 1–7* (see Table 1) to fit the experimental measurements. Table 2 presents the values obtained for the estimated parameters, and Fig. 9 presents the obtained results.

After the parameter estimation process with *stimuli 1–7*, we calculated the prediction for a qualitatively different stimulus (*stimulus 8*, Table 1), obtaining a satisfactory prediction, as shown in Fig. 9. Finally, based on the fits, we calculated the value of the angular size $\theta(t_\mathrm{peak} - \delta)$ when the maximum in the firing rate was produced (see the triangles in Fig. 9). The value obtained was 48.4 ± 2° (means ± SD), which is similar to the value that we obtained using the empirical method shown in Fig. 4.

By optimizing only the parameters values shown in the right part of Table 2, a satisfactory fit can be achieved throughout all dynamics of expansion, including the initial phasic responses (Fig. 9).

Table 2. *Estimated model parameters*

Parameter	Fitted Value (Means ± SD)
Max. normalized excitatory conductance	$g_\mathrm{e,max}/g_\mathrm{L} = 50 \pm 6$
Max. normalized inhibitory conductance	$g_\mathrm{i,max}/g_\mathrm{L} = 76 \pm 7$
Saturation 50% excitation	$T_{exc,50\%} = 0.12 \pm 0.02$
Saturation 50% inhibition	$T_\mathrm{inh,50\%} = 0.018 \pm 0.004$
LMC exponent	$a_\mathrm{LMC} = 0.4 \pm 0.2$
RF center displacement	$(\theta_\mathrm{c},\varphi_\mathrm{c}) = (5°,5°)$

Values were obtained by the method of least squares. The uncertainties of the parameters were estimated using the bootstrap method (means ± SD). Because the "maximum normalized excitatory and inhibitory conductance" were referred to the leak conductance, they are dimensionless (see *Eq. 15*). Also, the parameters $T_\mathrm{exc,50\%}$ and $T_\mathrm{inh,50\%}$ are dimensionless because they have the same unit than the $\mathrm{pre}(t)$ signal (see *Eq. 14*) and this signal was normalized by its maximum value for all stimuli. LMC, lamina monopolar cell; RF, receptive field.

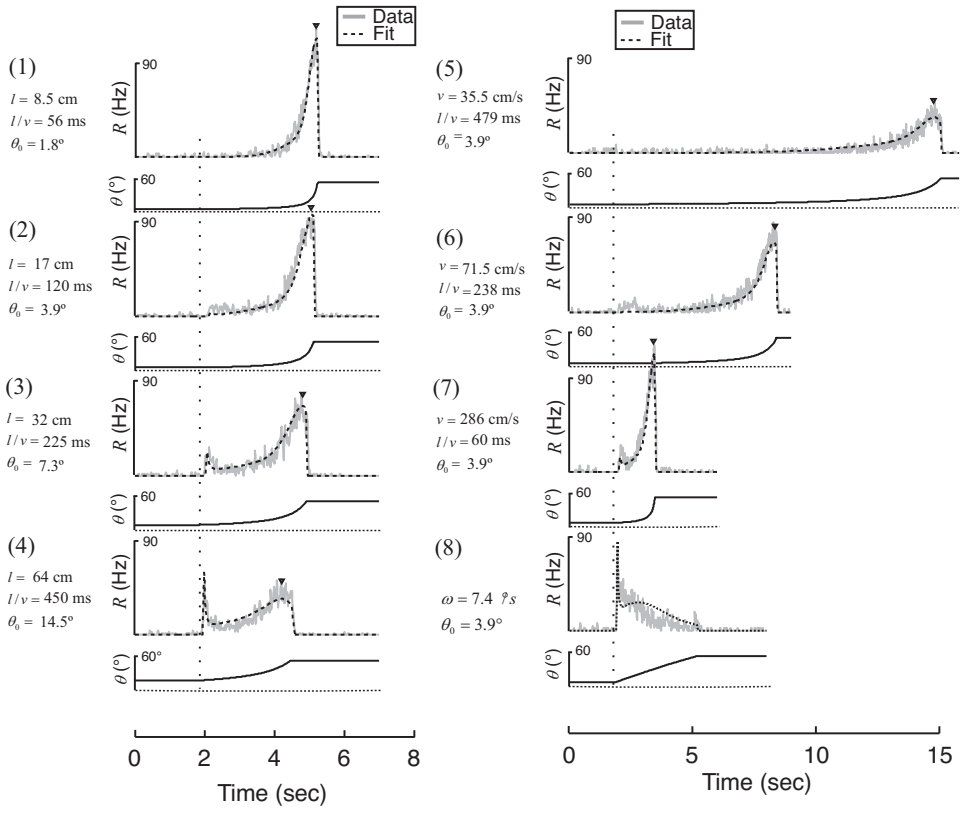

Fig. 9. Average data and model prediction of the firing rate of MLG1 neurons. *Left*: responses to *stimuli 1–4*. *Right*: responses to *stimuli 5–8*. Peristimulus time histograms (gray traces) show the mean spike rate from 8 MLG1 neurons with receptive fields mainly located over the right monitor (1 trial per stimulus, per neuron, per animal). Spikes were convolved with a 30-ms square kernel. The angular size, $\theta(t)$, of the looming object is represented by the black curved line at *bottom*. Dashed lines represent the firing rate predicted by the model. Dotted vertical lines signal the beginning of the stimulus expansion. Inverted black triangles signal the peak of firing according to the model. Finally, we calculated the prediction for a qualitatively different stimulus (*stimulus 8*), obtaining a satisfactory prediction (black dotted trace).

Angular Velocity Coding During the Looming Stimulus

The experimental results and proposed model demonstrate that similar to the LGMD of the locust, several biophysical processes likely operate in parallel to shape the visual response of MLG1 neurons in crabs. However, phenomenological descriptions of the response are also useful to correlate the activity of these neurons to the behavioral output of the animal. In such descriptions, neuronal activity (e.g., firing rate) is correlated with an optical variable, such as the angular size or angular velocity (Oliva 2013). Glantz (1974b) used this approach in crayfish and demonstrated the existence of motion detector neurons whose firing rate correlated with the angular velocity of looming stimuli. Given this previous result in crustaceans, we analyzed the relationship between the firing rate of MLG1 neurons and the stimulus angular velocity θ'. Figure 10*A* presents the average firing rate (gray traces) as a function of the stimulus angular velocity for *stimuli 1–7*. The black dotted lines are the model's prediction, which satisfactorily fits the entire range of responses.

There is a range of stimulation where the firing rate can be simply described as a function of the angular velocity only (Fig. 10*B*, black dotted lines). To illustrate this fact, we plotted the model prediction in the range of values of the angular increment $\Delta\theta(t) = \theta(t) - \theta_0$ from 3 to 35° (avoiding the initial transient responses that occur with large stimuli and the decline that occurs when the stimulus increases over a certain size). We computed the Pearson correlation coefficient between the measured and predicted firing rates and obtained a value of $\rho = 0.95$. We conclude that the firing rate of MLG1 neurons can be well described as a function of angular velocity in this range.

DISCUSSION

This study describes the response of crab MLG1 neurons to looming stimuli approaching from the ipsilateral side of the animal. We identified different physiological phenomena previously observed in other LSN neurons, such as the peak firing rate that occurs before collision (Figs. 3 and 7), the simultaneous action of excitatory and inhibitory synaptic currents (Figs. 2 and 5), a mapping between the filtered membrane potential and firing frequency (Fig. 6), a dependence of the excitation latency as a function of angular velocity (although with considerable data dispersion, Fig. 7), and phasic responses at the beginning of approach of large stimuli (Figs. 3 and 9). Based on the experimental results, we developed a plausible biophysical model of computation performed by these neurons to looming stimuli. Our model does not require the numerical integration of nonlinear differential equations associated with the spiking mechanism; it has the advantage of simplifying the description of the physiological mechanisms involved to assess their relative weight in the coding of looming stimuli.

Plausible Biophysical Model of Looming Detection in MLG1 Neurons

Based on the data obtained in this study, together with previous results from our group and previous research by other authors in the LGMD neuron, we propose a biologically plausible model of computation performed by the MLG1 neurons of crabs. The model proposes that each columnar channel provides information about the changes in luminosity for each ommatidium. This information is divided into excitatory and inhibitory synapses with different temporal dynamics. The actions of both synaptic conductances are added at the dendrite, which is modeled as a single compartment. The

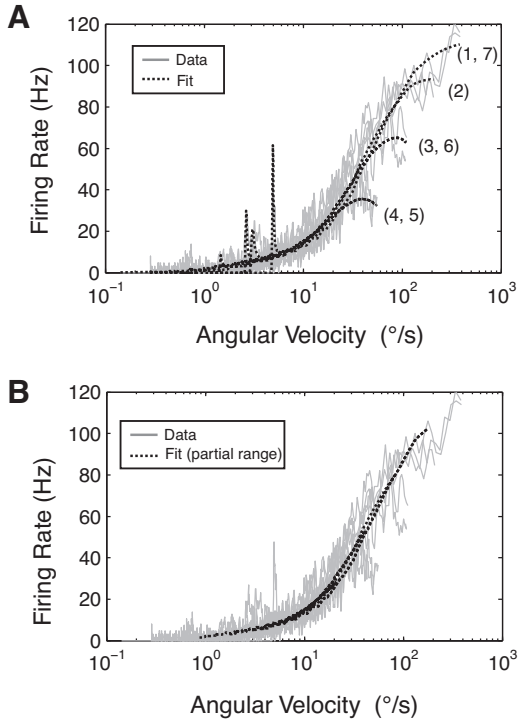

Fig. 10. Average and predicted firing rate as a function of the angular velocity, $\theta'(t)$. *A*: gray traces illustrate the average firing rate as a function of the angular velocity, $\theta'(t)$, from 8 MLG1 neurons that had receptive fields mainly located over the right monitor ($n = 8$, 1 trial per stimulus, per neuron, per animal). Spikes were convolved with a 30-ms square kernel. The black traces are the predictions of our model for the entire range of stimulation, $\theta \in [0,60°]$. The numbers inside the parentheses indicate the stimulus number. *B*: black dotted lines illustrate the model prediction in the range of values of the angular increment, $\Delta\theta \in [3°,35°]$. In this range, it is appropriate to assume that the firing rate of MLG1 neurons can be described as a function of the stimulus angular velocity.

dendrite changes its membrane potential as a function of the dynamic balance of the synaptic conductances. Similar to the model proposed for the locust LGMD (Jones and Gabbiani 2012), this process produces a dendritic sublinear transformation of the presynaptic signal (*Eqs. 14* and *15*). Finally, the dendritic potential becomes expansively transformed by the firing rate mechanism (*Eq. 8*).

Peak response of MLG1 neurons to looming stimuli. This feature is influenced by the balance among the dynamics of excitation, inhibition, and the receptive field size σ. MLG1 neurons have a receptive field of approximately $\sigma = 13°$ in the lateral visual field (Medan 2008), and our model simulations indicate that the peaks in the firing rate disappear for values of $\sigma > 18°$. Therefore, unlike LGMD, the relatively small receptive field of the MLG1 neuron is an important characteristic influencing the peak response.

Response of MLG1 neurons to expansion with constant angular velocity (stimulus 8). As shown in Fig. 9, the stimulus with a constant angular velocity expansion produces an initial phasic response and a subsequent reduction with increasing angular size $\theta(t)$. At first glance, this response is surprising because the object is approaching but the neuron does not increase its response. This result indicates that MLG1 neurons exhibit selectivity for expansions with increasing angular velocity. In our model, this selectivity is due to the joint action of synaptic excitation and inhibition. However, as shown in Fig. 9, the model prediction overestimates the neuronal response, likely because adaptation effects have not been considered (Peron and Gabbiani 2009).

In comparison to other studies on the coding of looming stimuli (e.g., Gabbiani et al. 1999), the proposed model was fitted to averaged neuronal responses, mainly due to the stimulation time constraint of the in vivo intracellular recording and habituation effects, which limited the possibility of high-frequency repeated stimulation. However, it is remarkable that the observed main features, including the initial phasic responses, the variable delay at the onset of stimulation, and the maximum firing rate before the end of the expansion, were observed in all measured neurons. Therefore, we believe that the model presented in this article possesses heuristic value to facilitate the understanding of the looming stimulus processing in a novel model system.

Possible Role of MLG1 Neurons in the Crab's Behavioral Responses to Looming Stimuli

Semiterrestrial crabs are common prey animals. *Neohelice* lives in estuarine ecosystems, where they form dense populations of burrow-centered, small home-range foragers. During low tide, they leave their burrows but keep them at a safe distance. In this situation, crabs display their activities in a flat, open environment, where they become vulnerable to predator attacks (crabs are an important food source for a number of seabirds, which catch them using a variety of hunting techniques; Iribarne and Martinez 1999). Under such predation pressure, it is essential to have a visual warning detection system that continuously reports to the animal about the emergence of approaching objects. The system of 14–16 MLG1 neurons in the crab (Sztarker et al. 2005; Medan 2008), with their sensitivity for looming stimuli (Oliva et al. 2007 and the results of this study) and their joint receptive fields encompassing the entire visual field of the crab's eye, are ideal candidates to play a central role in looming detection and avoidance responses. MLG1 neurons are thought to not only act as detecting looming elements but also to participate in the continuous control of the escape response, in which speed and direction are constantly adjusted based on the ongoing visual information (Nalbach 1990; Land and Layne 1995; Oliva and Tomsic 2012).

Regarding the regulation of the animal's speed, we have shown that the crab's escape response to looming stimuli consists of a threshold-type decision for initiating the escape run, followed by a visually regulated mechanism for the escape speed (Oliva and Tomsic 2012). The escape decision and regulated speed mechanism can be described by a phenomenological input-output function, where the crab's velocity, $v_c(t)$, is related to an optical variable resulting from the product of the angular increment since the onset of expansion, $\Delta\theta(t) = \theta(t) - \theta_0$, and the stimulus angular velocity, $\theta'(t)$. As shown in Fig. 10, MLG1 neurons are capable of reliably encoding the angular velocity of the stimulus until the stimulus reaches a size of ~35°, i.e., during the early stages of escape. However, our previous behavioral experiments (Oliva and Tomsic 2012) have shown that the animal's speed continues to grow almost until the end of the expansion. Therefore, if the MLG1 neurons are involved in the visuomotor transformation that controls the velocity of escape, the encoding of angular velocity when the

stimulus exceeds 35° may be accomplished by the combined computation performed by a number of neighboring MLG1 neurons. This possibility is reasonable because there is an important overlap between receptive fields of neighboring MLG1 elements in the lobula (Sztarker et al. 2005). In addition, the looming-sensitive MLG2 neuron, with its extensive receptive field, may also play a central role in the visuomotor transformation involved in the escape response to approaching objects (Oliva et al. 2007; Medan et al. 2007).

Regarding the control of the escape direction, crabs make continuous adjustments of their run direction as a function of the position of the threatening moving target. The maneuver employs two systems simultaneously. An open-loop mechanism directs the crab's translatory movements directly away from the stimulus and a rotational mechanism using continuous feedback turns the crab so that the stimulus is kept at 90° to the body axis, where escape is easiest (crabs run sideways) (Land and Layne 1995). This fine directional tuning requires a system of motion-sensitive neurons with differently oriented receptive fields, i.e., an array such as that provided by the ensemble of the MLG1 neurons found in *Neohelice* (Medan 2008).

Similarities and Differences in the Coding of the Looming Stimuli in Insects and Crustaceans

The visual nervous systems of insects and decapod crustaceans are thought to be homologous (Strausfeld 2005). They contain four retinotopic neuropils, known as the lamina, medulla, lobula, and lobula plate, and two connecting chiasmata (Sztarker et al. 2005). At the level of the first and simplest neuropil, the lamina, similar neuronal identities can be recognized between insects and crustaceans (Sztarker et al. 2009). At the level of the third neuropil, motion-sensitive neurons with large tangential processes that collect information from extensive parts of the retinotopic mosaic and with axons projecting to the midbrain are also elements common to insects and crustaceans (e.g., Rind 1987; Yamawaki and Toh 2003; Medan et al. 2007). In both insects and crustaceans, the motion-sensitive neurons of the lobula display habituation to repeated object motion (Gray 2005; Tomsic et al. 2003). Given the homology of the visual system and the similarities in the general morphology and response characteristics of giant neurons of the lobula, it is interesting to compare the way in which the LSN neurons of insects and crustaceans respond to approaching objects. The results of the present study demonstrate that in many respects the MLG1 neuron of the crab behaves similar to the locust LGMD: *1*) The response to looming stimuli appears to be strongly influenced by a dynamic balance between synaptic excitation and inhibition, *2*) there is a phasic component of responses at the beginning of the stimulus expansion, *3*) the peak firing rate occurs before the end of expansion, *4*) the response delay depends on the stimulus angular velocity, and *5*) there is a mapping between the membrane potential depolarization and firing rate. Despite these similarities, crab MLG1 neurons and the locust LGMD differ in some important aspects. In the locust, there is only one bilateral pair of LGMD neurons (as would be the case for the MLG2 of the crab, Medan et al. 2007), with each neuron covering the entire view of the eye ipsilateral to its lobula projections. In contrast, the MLG1 class of the crab comprises 14–16 bilateral pairs, with smaller receptive fields that are distributed over the extensive visual field of the crab's eye. In this regard and based on the results of our model, an important difference is that the peak of activity of individual MLG1 neurons appears to be mainly influenced by the size of the receptive field. Assuming that the system of MLG1 neurons of the crab, similar to the LGMD of the locust, participates in the detection of approaching objects and collision avoidance behaviors, it is tempting to speculate about the differences between the two looming-sensitive systems and the characteristics of the behaviors with which they are involved. To date, there is no compelling behavioral evidence that the avoidance response to looming stimuli in the locust is highly directionally tuned. During flight looming stimuli may elicit different avoidance behaviors, such as a gliding response with no apparent directional component (Santer et al. 2005a) or changes of the trajectory that unpredictably bank the animal away or towards the stimulus (Chan and Gabbiani 2013; Mcmillan et al. 2013). On the other hand, the jumping response is performed to the opposite site of the approaching stimulus, but the direction is not finely tuned (Fotowat and Gabbiani 2007; Santer et al. 2005b). Thus, based on current behavioral results, the degree of directionality implicated in the locust avoidance responses can be sufficiently performed with a coarse control system, such as the one provided by the single pair of LGMD neurons. In crabs, however, behavioral experiments have demonstrated the existence of finely tuned directional control systems (see *Possible Role of MLG1 Neurons in the Crab's Behavioral Responses to Looming Stimuli*) (e.g., Land and Layne 1995). These controls cannot be achieved with a single pair of bilateral neurons but can instead be suitably accomplished with a neuronal ensemble, as formed by the MLG1 neurons.

ACKNOWLEDGMENTS

We thank Dr. Ines Samengo for comments on the manuscript.

GRANTS

This work was supported by Agencia Nacional de Promoción Científica y Tecnológica (ANPCYT) Grant PICT 2012-2765 (to D. Oliva) and Universidad de Buenos Aires Grant W888 and ANPCYT Grant PICT 2010-1016 (to D. Tomsic).

DISCLOSURES

No conflicts of interest, financial or otherwise, are declared by the author(s).

AUTHOR CONTRIBUTIONS

Author contributions: D.O. and D.T. conception and design of research; D.O. performed experiments; D.O. analyzed data; D.O. and D.T. interpreted results of experiments; D.O. prepared figures; D.O. and D.T. drafted manuscript; D.O. and D.T. edited and revised manuscript; D.O. and D.T. approved final version of manuscript.

REFERENCES

Berón de Astrada M, Tomsic D. Physiology and morphology of visual movement detector neurons in a crab (Decapoda: Brachyura). *J Comp Physiol A Neuroethol Sens Neural Behav Physiol* 188: 539–551, 2002.

Berón de Astrada M, Medan V, Tomsic D. How visual space maps in the optic neuropils of a crab. *J Comp Neurol* 519: 1631–1639, 2011.

Berón de Astrada M, Bengochea M, Medan V, Tomsic D. Regionalization in the eye of the grapsid crab Neohelice granulata (=Chasmagnathus granulatus): variation of resolution and facet diameters. *J Comp Physiol A Neuroethol Sens Neural Behav Physiol* 198: 173–180, 2012.

Borst A. Fly visual interneurons responsive to image expansion. *Zool Jb Physiol* 95: 305–313, 1991.

Card GM. Escape behaviors in insects. *Curr Opin Neurob* 22: 180–186, 2012.

Chan RW, Gabbiani F. Collision-avoidance behaviors of minimally restrained flying locusts to looming stimuli. *J Exp Biol* 216: 641–55, 2013.

Destexhe A, Mainen ZF, Sejnowski TJ. An efficient method for computing synaptic conductances based on a kinetic model of receptor binding. *Neural Comput* 6: 14–18, 1994.

Fotowat H, Fayyazuddin A, Bellen HJ, Gabbiani F. A novel neuronal pathway for visually guided escape in Drosophila melanogaster. *J Neurophysiol* 102: 875–885, 2009.

Fotowat H, Gabbiani F. Relationship between the phases of sensory and motor activity during a looming evoked multistage escape behavior. *J Neurosci* 27: 10047–10059, 2007.

Fotowat H, Gabbiani F. Collision detection as a model for sensory-motor integration. *Annu Rev Neurosci* 34: 1–19, 2011.

Gabbiani F, Mo C, Laurent G. Invariance of angular threshold computation in a wide-field looming sensitive neuron. *J Neurosci* 21: 314–329, 2001.

Gabbiani F, Krapp HG, Koch C, Laurent G. Multiplicative computation in a visual neuron sensitive to looming. *Nature* 21: 320–324, 2002.

Gabbiani F, Krapp HG, Laurent G. Computation of object approach by a wide-field, motion-sensitive neuron. *J Neurosci* 19: 1122–1141, 1999.

Glantz RM. Defense reflex and motion detector responsiveness to approaching targets: the motion detector trigger to the defense reflex pathway. *J Comp Physiol A Neuroethol Sens Neural Behav Physiol* 95: 297–314, 1974a.

Glantz RM. Habituation of the motion detectors of the crayfish optic nerve: their relationship to the visually evoked defense reflex. *J Neurobiol* 5: 489–510, 1974b.

Gray JR. Habituated visual neurons in locusts remain sensitive to novel looming objects. *J Exp Biol* 208: 2515–2532, 2005.

Gray JR, Blincow E, Robertson RM. A pair of motion-sensitive neurons in the locust encode approaches of a looming object. *J Comp Physiol A Neuroethol Sens Neural Behav Physiol* 196: 927–938, 2010.

Herberholz J, Marquart G. Decision making and behavioral choice during predator avoidance. *Front Neurosci* 6: 1–15, 2012.

Hemmi JM. Predator avoidance in fiddler crabs: 1. Escape decisions in relation to the risk of predation. *Animal Behav* 69: 603–614, 2005a.

Hemmi JM. Predator avoidance in fiddler crabs: 2. The visual cues. *Animal Behav* 69: 615–625, 2005b.

Hemmi JM, Tomsic D. The neuroethology of escape in crabs: from sensory ecology to neurons and back. *Curr Opin Neurobiol* 22: 194–200, 2012.

Iribarne OO, Martinez MM. Predation on the southwestern Atlantic fiddler crab (Uca uruguayensis) by migratory shorebirds (Pluvialis dominica, P. squatarola, Arenaria interpres, and Numenius phaeopus). *Estuaries* 22: 47–54, 1999.

Jones PW, Gabbiani F. Synchronized neural input shapes stimulus selectivity in a collision-detecting neuron. *Curr Biol* 20: 2052–2057, 2010.

Jones PW, Gabbiani F. Logarithmic compression of sensory signals within the dendritic tree of a collision-sensitive neuron. *J Neurosci* 32: 4923–4934, 2012.

Krapp HG, Gabbiani F. Spatial distribution of inputs and local receptive field properties of a wide-field, looming sensitive neuron. *J Neurophysiol* 93: 2240–2253, 2005.

Land M, Layne J. The visual control of behaviour in fiddler crabs. *J Comp Physiol A Neuroethol Sens Neural Behav Physiol* 177: 91–103, 1995.

Laughlin SB, Hardie RC. Comon strategies for light adaptation in the peripheral visual systems of fly and dragonfly. *J Comp Physiol A Neuroethol Sens Neural Behav Physiol* 128: 319–340, 1978.

Layne J, Wicklein M, Dodge FA, Barlow RB. Prediction of maximum allowable retinal slip speed in the fiddler crab, Uca pugilator. *Biol Bull* 193: 202–203, 1997.

McMillan GA, Loessin V, Gray JR. Bilateral flight muscle activity predicts wing kinematics and 3-dimensional body orientation of locusts responding to looming objects. *J Exp Biol* 216: 3369–3380, 2013.

Medan V, Oliva D, Tomsic D. Characterization of lobula giant neurons responsive to visual stimuli that elicit escape behaviors in the crab Chasmagnathus. *J Neurophysiol* 98: 2414–2428, 2007.

Medan V. Caracterización morfológico-funcional de neuronas sensibles al movimiento involucradas en comportamientos visuales del cangrejo Chasmagnathus (PhD Thesis). Buenos Aires, Argentina: Facultad de Ciencias Exactas y Naturales, Universidad de Buenos Aires, 2008. http://digital.bl.fcen.uba.ar/Download/Tesis/Tesis_4323_Medan.pdf.

Nalbach HO. Visually elicited escape in crabs. In: *Frontiers in Crustacean Neurobiology*, edited by Wiese K, Krenz WD, Tautz J, Reichert H, Mulloney B. Basel, Switzerland: Basel, 1990.

Oliva D, Medan V, Tomsic D. Escape behavior and neuronal responses to looming stimuli in the crab Chasmagnathus granulatus (Decapoda: Grapsidae). *J Exp Biol* 210: 865–880, 2007.

Oliva D. Mecanismos de detección visual y evitación de colisiones en un nuevo modelo experimental, el cangrejo Chasmagnathus granulatus (Online). Buenos Aires, Argentina: Facultad de Ciencias Exactas y Naturales, Universidad de Buenos Aires, 2010. http://digital.bl.fcen.uba.ar/Download/Tesis/Tesis_4678_Oliva.pdf.

Oliva D, Tomsic D. Visuo-motor transformations involved in the escape response to looming stimuli in the crab Neohelice (=Chasmagnathus) granulata. *J Exp Biol* 215: 3488–3500, 2012.

Oliva D. Collision avoidance models. In: *Encyclopedia of Computational Neuroscience: SpringerReference*, edited by Jaeger D, Jung R. Berlin, Heidelberg: Springer-Verlag, 2013.

O'Shea M, Rowell CH. Protection from habituation by lateral inhibition. *Nature* 254: 53–55, 1975.

Peron SP, Gabbiani F. Spike frequency adaptation mediates looming stimulus selectivity in a collision detecting neuron. *Nat Neurosci* 12: 318–326, 2009.

Rind FC. Non-directional, movement sensitive neurons of the locust optic lobe. *J Comp Physiol A Neuroethol Sens Neural Behav Physiol* 161: 477–494, 1987.

Rind FC, Simmons PJ. Orthopteran DCMD neuron: a reevaluation of responses to moving objects. I. Selective responses to approaching objects. *J Neurophysiol* 68: 1654–1666, 1992.

Rind FC, Bramwell DI. Neural network based on the input organization of an identified neuron signaling impending collision. *J Neurophysiol* 75: 967–985, 1996.

Rind FC, Simmons PJ. Seeing what is coming: building collision sensitive neurones. *Trends Neurosci* 22: 215–220, 1999.

Rowell CH, O'Shea M, Williams JL. The neuronal basis of a sensory analyser, the acridid movement detector system. IV. The preference for small field stimuli. *J Exp Biol* 68: 157–185, 1977.

Santer RD, Simmons PJ, Rind FC. Gliding behaviour elicited by lateral looming stimuli in flying locusts. *J Comp Physiol A Neuroethol Sens Neural Behav Physiol* 191: 61–73, 2005a.

Santer RD, Yamawaki Y, Rind FC, Simmons PJ. Motor activity and trajectory control during escape jumping in the locust Locusta migratoria. *J Comp Physiol A Neuroethol Sens Neural Behav Physiol* 191: 965–975, 2005b.

Schlotterer GR. Response of the locust descending movement detector neuron to rapidly approaching and withdrawing visual stimuli. *Can J Zool* 55: 1372–1376, 1977.

Srinivasan MV, Zhang S. Visual motor computations in insects. *Annu Rev Neurosci* 27: 679–696, 2004.

Strausfeld NJ. The evolution of crustacean and insect optic lobes and the origins of chiasmata. *Arthropod Struct Dev* 34: 235–256, 2005.

Sztarker J, Tomsic D. Binocular visual integration in the crustacean nervous system. *J Comp Physiol A Neuroethol Sens Neural Behav Physiol* 190: 951–962, 2004.

Sztarker J, Strausfeld NJ, Tomsic D. Organization of optic lobes that support motion detection in a semiterrestrial crab. *J Comp Neurol* 493: 396–411, 2005.

Sztarker J, Tomsic D. Neuronal correlates of the visually elicited escape response of the crab Chasmagnathus upon seasonal variations, stimuli changes and perceptual alterations. *J Comp Physiol A Neuroethol Sens Neural Behav Physiol* 194: 587–596, 2008.

Sztarker J, Strausfeld N, Andrew D, Tomsic D. Neural organization of first optic neuropils in the littoral crab Hemigrapsus oregonensis and the semiterrestrial species Chasmagnathus granulatus. *J Comp Neurol* 513: 129–150, 2009.

Sztarker J, Tomsic D. Brain modularity in arthropods: individual neurons that support "what" but not "where" memories. *J Neurosci* 31: 8175–8180, 2011.

Tammero LF, Dickinson MH. Collision-avoidance and landing responses are mediated by separate pathways in the fruit fly Drosophila melanogaster. *J Exp Biol* 205: 2785–2798, 2002.

Tomsic D, Berón de Astrada M, Sztarker J. Identification of individual neurons reflecting short- and long-term visual memory in an arthropod. *J Neurosci* 23: 8539–8546, 2003.

Wasserman L. *All of Statistics: a Concise Course in Statistical Inference*. Berlin, Heidelberg: Springer, 2004, chapt 8, p 107–110.

Weber F, Machens CK, Borst A. Spatiotemporal response properties of optic-flow processing neurons. *Neuron 67*: 629–642, 2010.

Wiersma CA, Roach JL, Glantz RM. Neural integration in the optic system. In: *The Biology of the Crustacea, Vol 4. Neural Integration and Behavior*, edited by Sandeman DC, Atwood HL. New York: Academic, 1982.

Yamawaki Y, Toh Y. Response properties of visual interneurons to motion stimuli in the praying mantis, Tenodera aridifolia. *Zool Sci* 20: 819–832, 2003.

Yamawaki Y, Toh Y. Responses of descending neurons to looming stimuli in the praying mantis Tenodera aridifolia. *J Comp Physiol A Neuroethol Sens Neural Behav Physiol* 195: 253–264, 2009.